JACS
JOURNAL OF THE AMERICAN CHEMICAL SOCIETY
Article
pubs.acs.org/JACS

Mapping the Nucleotide Binding Site of Uncoupling Protein 1 Using Atomic Force Microscopy

Rong Zhu,[†,§] Anne Rupprecht,[‡,§] Andreas Ebner,[†] Thomas Haselgrübler,[∥] Hermann J. Gruber,[†] Peter Hinterdorfer,[†] and Elena E. Pohl*[,‡,§]

[†]Institute for Biophysics, Johannes Kepler University, Linz, Austria
[‡]Institute of Physiology, Pathophysiology and Biophysics, University of Veterinary Medicine, Vienna, Austria
[§]Institute of Cell Biology and Neurobiology, Charité−Universitaetsmedizin, Berlin, Germany
[∥]Center for Advanced Bioanalysis GmbH, Linz, Austria

Supporting Information

ABSTRACT: A tight regulation of proton transport in the inner mitochondrial membrane is crucial for physiological processes such as ATP synthesis, heat production, or regulation of the reactive oxygen species as proposed for the uncoupling protein family members (UCP). Specific regulation of proton transport is thus becoming increasingly important in the therapy of obesity and inflammatory, neurodegenerative, and ischemic diseases. We and other research groups have shown previously that UCP1- and UCP2-mediated proton transport is inhibited by purine nucleotides. Several hypotheses have been proposed to explain the inhibitory effect of ATP, although structural details are still lacking. Moreover, the unresolved mystery is how UCP operates in vivo despite the permanent presence of high (millimolar) concentrations of ATP in mitochondria. Here we use the topographic and recognition (TREC) mode of an atomic force microscope to visualize UCP1 reconstituted into lipid bilayers and to analyze the ATP−protein interaction at a single molecule level. The comparison of recognition patterns obtained with anti-UCP1 antibody and ATP led to the conclusion that the ATP binding site can be accessed from both sides of the membrane. Using cantilever tips with different cross-linker lengths, we determined the location of the nucleotide binding site inside the membrane with 1 Å precision. Together with the recently published NMR structure of a UCP family member (Berardi et al. Nature, 2011, 476, 109−113), our data provide a valuable insight into the mechanism of the nucleotide binding and pave the way for new pharmacological approaches against the diseases mentioned above.

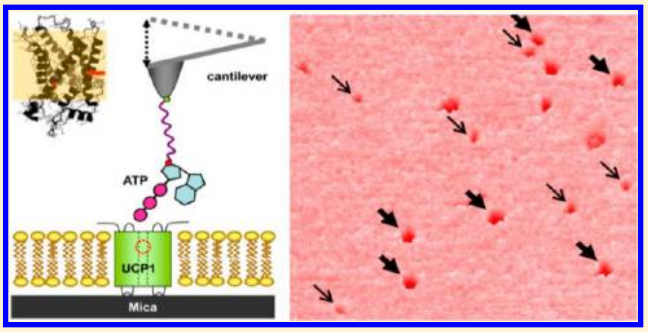

INTRODUCTION

The main source of ATP in aerobic organisms is oxidative phosphorylation. The chemiosmotic theory of Mitchell[1] predicts that a proton leak in the inner mitochondrial membrane, not coupled to ATP synthesis, would cause the uncoupling of respiration. It is obvious that uncoupling (e.g., mediated by the mitochondrial subfamily of uncoupling proteins, UCP) decreases the efficiency of ATP synthesis and can become toxic to the cell if not tightly regulated.

Uncoupling protein 1 (UCP1), the best studied representative of the mitochondrial uncoupling protein subfamily, is mainly localized in brown adipose tissue and dissipates the energy of the electrochemical gradient over the inner mitochondrial membrane as heat, enabling nonshivering thermogenesis.[2] Because this process prevents energy storage as fat, UCP1 has been proposed as a pharmaceutical target for the treatment of obesity[3,4] alternatively to the artificial uncoupler dinitrophenol. The latter was extensively used in diet pills as long ago as the 1930s but turned out to be dangerous, mainly because of its narrow regulatory window.[5] Current research is concentrated on the regulation of UCP1, which was also naturally found in adults[6] and acts similarly to dinitrophenol with regard to the treatment of obesity.[7]

Most research groups now agree that long chain fatty acids (FA) activate UCP1, whereas the binding of purine nucleotides (PN) results in the inhibition of UCP1's proton transporting activity.[8−12] However, neither the mechanism of activation nor that of nucleotide-mediated inhibition is known at a structural level (reviewed in refs 13 and 14). Moreover, it remains unclear how UCP1 operates in vivo in spite of the permanent presence of millimolar concentrations of ATP in mitochondria. To address these issues we have proposed that high membrane potential can potentiate the activation mediated by FA, overriding the inhibition by nucleotides.[15] Another hypothesis, which we test in this work, is that under certain circumstances PN are able to bind to the protein binding site without inhibiting it.

Received: December 23, 2012

   dx.doi.org/10.1021/ja312550k | J. Am. Chem. Soc. XXXX, XXX, XXX−XXX

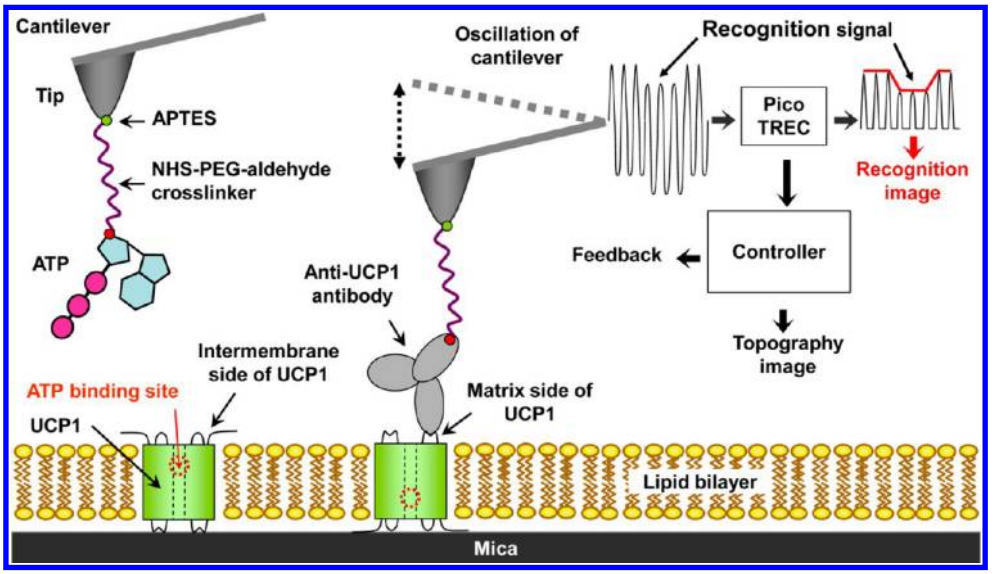

Figure 1. The experimental setup showing the uncoupling protein 1 (UCP1) reconstituted into lipid bilayer formed on a mica surface and a cantilever tip functionalized by antibody or ATP and used for measurements in the recognition mode.

The existing models for UCP1 inhibition are largely based on the chemical binding of covalently labeled ATP derivatives and site-directed mutagenesis.[13,14,16,17] Published data are not entirely consistent, although several common features are apparent: (i) tri- and diphosphates, but not monophosphates, bind to UCP1; (ii) nucleotides are regarded as strictly allosteric inhibitors of UCP; (iii) inhibition does not depend on the concentration of fatty acids and is not voltage-gated; (iv) three arginine residues (R83, R182, R276), which are conserved in the UCP homologues, are crucial for nucleotide binding and inhibition; (v) a conformational change occurs after binding that inhibits the transport activity of the UCP1; and (vi) in contrast to the ANT carrier, ATP can access the UCP1 binding site only from the cytosolic side (c-side).

In the absence of a crystallographic structure for UCP1, no further structural details or mechanistic insights have emerged in the last decades. The recently published NMR structure of UCP2,[18] with 57% homology to UCP1, unexpectedly revealed that the central pore of UCP2 is even larger than that of another ATP/ADP-binding mitochondrial protein, ANT. Using GDP labeled with NO, the authors showed that the nucleotide binds deeply within the UCP2 channel, similarly to the binding of ADP shown previously for ANT.[19] The finding raises doubts over the existence of the separate ATP binding pocket[14,17] and implies that the pore may be involved in binding of PN to UCP1.[18]

We have used the TREC mode of high-resolution atomic force microscopy to obtain topography and recognition images simultaneously, thereby allowing detailed mechanistic and structural insights into the process of nucleotide binding. We aimed (i) to visualize antibody and nucleotide interactions with UCP1, (ii) to evaluate whether ATP may bind from both cis and trans sides to the protein, and (iii) to calculate the localization of the putative nucleotide binding site inside the membrane.

RESULTS

To form a bilayer membrane for characterization by AFM, we incubated proteoliposomes reconstituted with purified UCP1 on mica (Figure 1). In the parallel electrophysiological experiments shown in Figure 3 in ref 15 we ensured that the protein is functionally active, i.e., it can be activated with arachidonic acid and inhibited by ATP as shown previously.[12] We obtained AFM images by scanning with a sharp tip, mounted to a soft cantilever spring, over the surface of a sample in the x and y directions to probe the topography of the surface. Using five topographical images of protein from independent preparations, we calculated the average protein density as $(60 \pm 16)/\mu m^2$.

We further performed experiments in which the cantilever was functionalized with an antibody specific to amino acid residues 145−159 of UCP1 (anti-UCP1 AB, Figure 1). In these experiments, only about half of the protein molecules detected in the topographic image were accessible by the antibody tethered to the tip, so that they gave rise to recognition signals (Figure 2). The ratio of recognized to unrecognized proteins in several experiments was 54:33. This result confirms that the orientation of protein in the planar bilayer is random, as would be expected. The specificity of antibody−protein interactions was proved by addition of the peptide blocking UCP1 antibody (Experimental Section, Figure 2). AFM images taken 22 and 44 min after the addition of antibody demonstrate an increasing amount of unrecognized proteins. After 44 min, nearly all UCP1 binding sites for antibodies remained free. No recognition signals were measured in bilayer membranes without UCP1 (Figure S1, Supporting Information).

To characterize the UCP1−ATP interaction, the cantilever tip was functionalized with ATP (Figure 1). The comparison of the topographic and recognition images revealed that all spots that were detected topographically (Figure 3A) were recognized by the ATP-functionalized tip (Figures 3B and 4A). The recognition spots disappeared when ATP at a final concentration of 4.8 mM was injected into the buffer solution, demonstrating the specific character of the interaction (Figure 4B). After ATP had been washed out, the recognition spots were again detected (Figure 4C). The almost 100% recognition of UCP1 by ATP is surprising because of the random orientation of the protein (Figure 2); i.e., ATP was anticipated to bind to only about 50% of all spots. Recognition of all UCP-binding sites by ATP implies that the nucleotide binding sites

dx.doi.org/10.1021/ja312550k | J. Am. Chem. Soc. XXXX, XXX, XXX−XXX

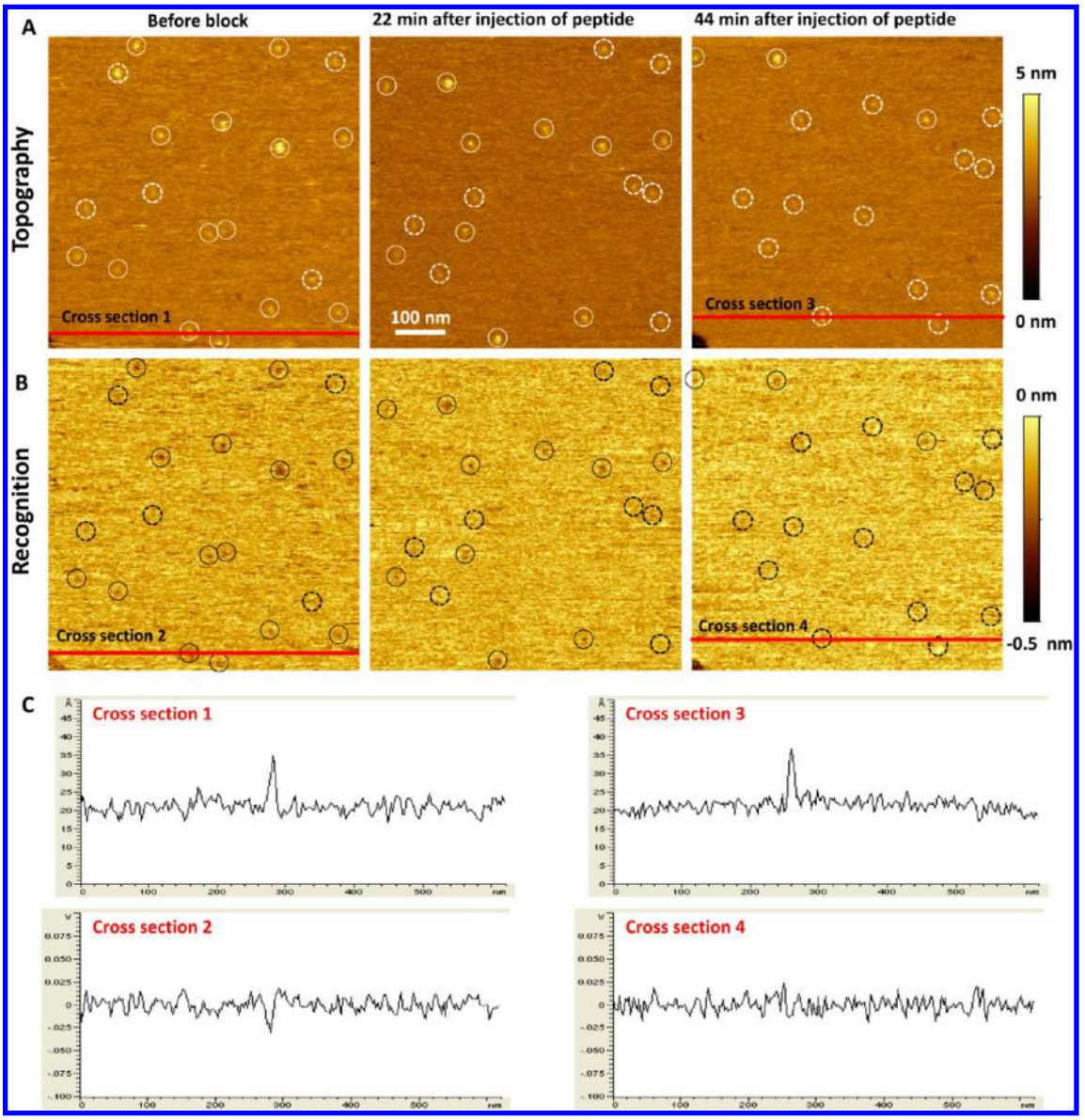

Figure 2. High-resolution topographical (A) and UCP1 antibody-recognition (B) images of UCP1 reconstituted into a bilayer membrane. Solid and dashed circles indicate recognized and unrecognized protein molecules, respectively. Before blocking, 14 proteins are recognized and 5 proteins are not. After 44 min, nearly all molecules are blocked. (C) Cross-section images before (1,2) and after (3,4) blocking.

are accessible from both sides. In contrast, results obtained with isolated mitochondria and proteoliposomes are consistent with the unilateral binding of nucleotides to UCP1 from the cytosolic side in mitochondria.[10,20] However, no direct evidence is available. For another member of the mitochondrial carrier family with a high degree of homology to UCP, the ADP/ATP carrier (ANT), it has been hypothesized that a single binding site for nucleotides and inhibitors may be alternately open to the matrix and to the cytosol during the transport process.[21] As shown in our experiments, the recognition of all UCP1 molecules by ATP molecules on rapidly oscillating tips rules out the presence of low-affinity binding sites reacting on a time scale of minutes, as suggested from experiments with mitochondria.[22]

Figure 3 provides further insights into the process of ATP–protein binding. Whereas the size of protein spots in the topographic image was uniform (Figure 3A,C), the size of recognition spots appeared different (Figure 3B,D). Two groups with mean diameters of 12.65 ± 1.03 and 17.68 ± 0.86 nm were determined (Figure 3D). Given that the ATP binding site can be reached from both sides, the existence of two different sizes of recognition spot may be explained by differences in submersion depths of the linker (Figure 5A,B). To estimate the localization of the binding site, the data from six tips differing in the length of their ATP linkers were analyzed (Figure 5C). For tip 1, the linker was so short that the ATP could only reach the binding site from one side of the UCP1 (Figure 6, Table 1), which supports two possible orientations of UCP1 in the lipid bilayer on the mica. For tips 2–6, the effective lengths of cross-linkers were 6.5, 7.8, 8.2, 8.0, and 11.2 nm, respectively (Table 1). For each tip, the difference in the diameter of large recognition spots, D_b, and small recognition spots, D_s, was found to be similar, with an average value of 4.84 ± 0.12 nm. The depth of the ATP binding site in UCP1 (x) was calculated using the following equation

dx.doi.org/10.1021/ja312550k | J. Am. Chem. Soc. XXXX, XXX, XXX–XXX

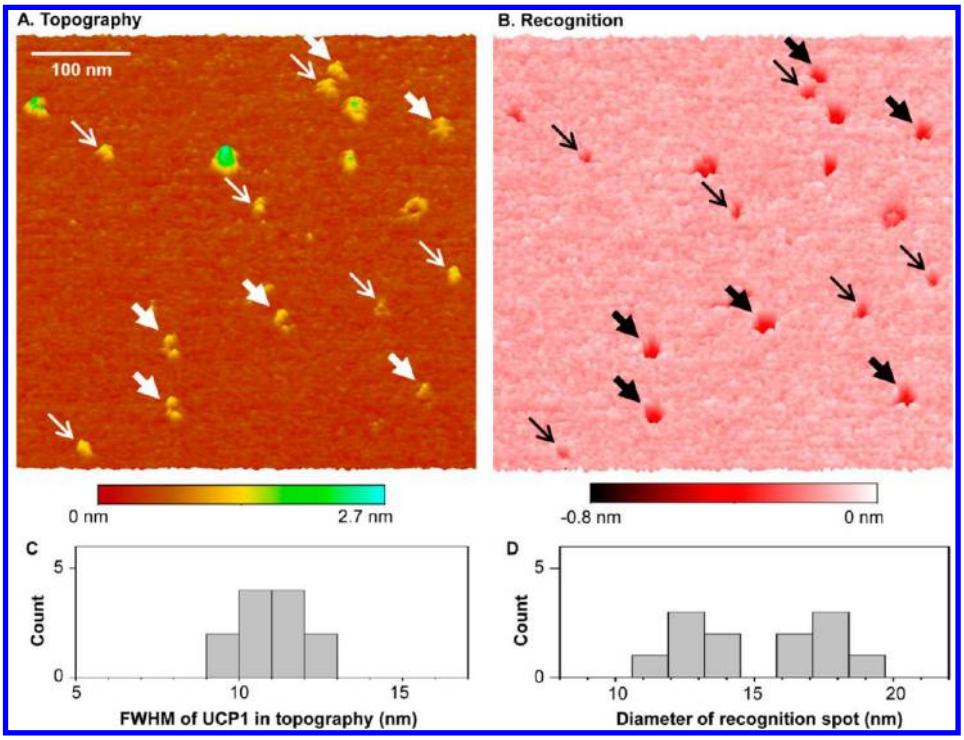

Figure 3. High-resolution topographical (A) and ATP-recognition (B) images of UCP1 reconstituted into a bilayer membrane. In the recognition image (B) large (thick arrows) and small (thin arrows) spots are distinguished. The corresponding molecules in image A are homogeneous in size. Rarely occurring large aggregates (not marked) were not considered further. (C) Statistical distribution of size of protein molecules, fwhm (full width half-maximum), in the topography image. (D) Statistical distribution of the diameter of the recognition spots.

$$x = \frac{1}{2}(d - (R_b - R_s) - (H_b - H_s))$$

where d is the thickness of the bilayer membrane (5 nm, Figure S2, Supporting Information), R_b and R_s are the radii of the large and small recognition spots, and H_b and H_s are the heights of the intermembrane and the matrix sides of the UCP1, respectively (Figure 6). $R_b - R_s$ is the distance between the binding site according to the orientation of the protein in the bilayer. We calculated x as 1.27 ± 0.10 nm from the average of five tips (Table 1).

The height of UCP1 can be roughly estimated from the measurements of protein height above the membrane (H_b, H_s in Table 1) and the membrane thickness (5 nm, Figure S2, Supporting Information). This value is ~7.31 nm. According to molecular dynamics simulation studies and structural studies,[18,23,24] the height of homologous mitochondrial proteins ANT and UCP2 is calculated to be approximately 6 nm, which is in good agreement with our estimation for UCP1.

■ DISCUSSION

Despite immense efforts from many research groups working on mitochondrial anion carriers, structural information about these membrane proteins is scarce.[25−28] To date, structural data are available for only two proteins, the ANT[19] and uncoupling protein 2.[18] The exploration of the uncoupling proteins is difficult because of their high hydrophobicity and because of difficulties with the production of functional recombinant proteins, protein crystals, and reliable antibodies. In the present work, we show that the comparison of images taken simultaneously by topographic and recognition signals of an atomic force microscope (TREC imaging mode) can provide valuable structural information. Using AFM tips functionalized with ATP and of different effective cross-linker lengths we show for the first time that (i) ATP binds from both sides to the uncoupling protein and (ii) the binding site is localized at a distance of 1.27 ± 0.10 nm from the membrane surface.

In the absence of the molecular structure of UCP1, the crystallographic structure of ANT (21% homology to UCP1) and the recently published NMR structure of UCP2 (57% homology to UCP1[18,19]) are very useful for the structural interpretation of our data. The homologies between ANT, UCP2, and UCP1 imply that these proteins could share common features in their interaction with nucleotides.[16] Molecular dynamic simulations performed for ANT revealed a spontaneous binding of ADP to the deeply positioned binding sites within the protein pore.[23,24] Wang and Tajkhorshid provided evidence that (i) "an unusually strong positive electrostatic potential in the lumen of ANT may be the main driving force for the observed spontaneous binding of ADP" and (ii) "it is likely a common attribute among the entire family of mitochondrial carriers".[24] This study suggested that two regions of charged residues localized several angstroms apart are involved in ADP binding in ANT (Figure 3 in ref 24). Comparison of these regions with the corresponding amino acids in UCP1 and UCP2 reveals a high degree of conservation, suggesting that the binding sites have similar locations in all three mitochondrial proteins. Moreover, residues R79 and R279 correspond to the arginines involved in nucleotide binding and protein inhibition in UCP1. According to the three-step binding model proposed for UCP1,[17] β-phosphate of PN binds first to R182 (helix IV, loose binding). The second step is the binding of γ-phosphate to R83 after protonation of E190 (tight binding). After the subsequent binding of α-phosphate to R276 (helix VI) the protein switches to the inhibited conformation. Modeling of UCP1 based on the NMR

dx.doi.org/10.1021/ja312550k | J. Am. Chem. Soc. XXXX, XXX, XXX−XXX

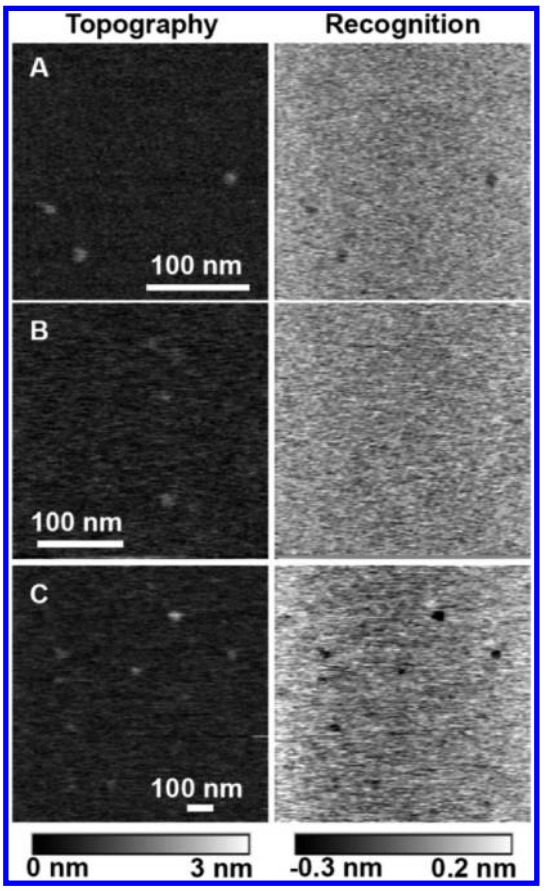

Figure 4. Specificity of UCP1 blocking by ATP. Topographic and recognition images before blocking of UCP1 by ATP (A), after UCP1 blocking by ATP (B), and after washing out of ATP (C).

structure of UCP2 (Figure 7A,B) shows that R182 protrudes into the central pore and may be responsible for the initial binding of UCP1. Its position may correspond to the distance of the binding site from the surface, approximately 1.27 nm, calculated in this study (Figure 6, Table 1).

In contrast to the studies of the Klingenberg and Garlid groups, our experimental data support the structural data of Berardi et al.,[18] which demonstrated that nitroxide-labeled GDP binds inside the central pore similarly to ADP binding to ANT. We further hypothesize that only binding from the c-side (Figure 7C) would lead to the conformational change in the protein and thus to inhibition (Figure 7D). PN binding from the m-side does not induce the conformational change and thus hinders protein inhibition because no binding from the c-side is possible (Figure 7E). This suggestion would plausibly explain one of the unresolved bioenergetical questions: how can the protein be in the active state despite the presence of millimolar ATP concentrations in the cytosol?

■ CONCLUSIONS

High-resolution topographical AFM images allowed us for the first time to visualize uncoupling proteins reconstituted into bilayer membranes. Simultaneously measured recognition images reveal the existence of a single ATP binding site that can be accessed by nucleotides from both sides. Considering the experimental data in the light of structural data on UCP1 and ANT, it is likely that there is a second charged ring in UCP1 situated at the bottom of the vestibule. In the absence of

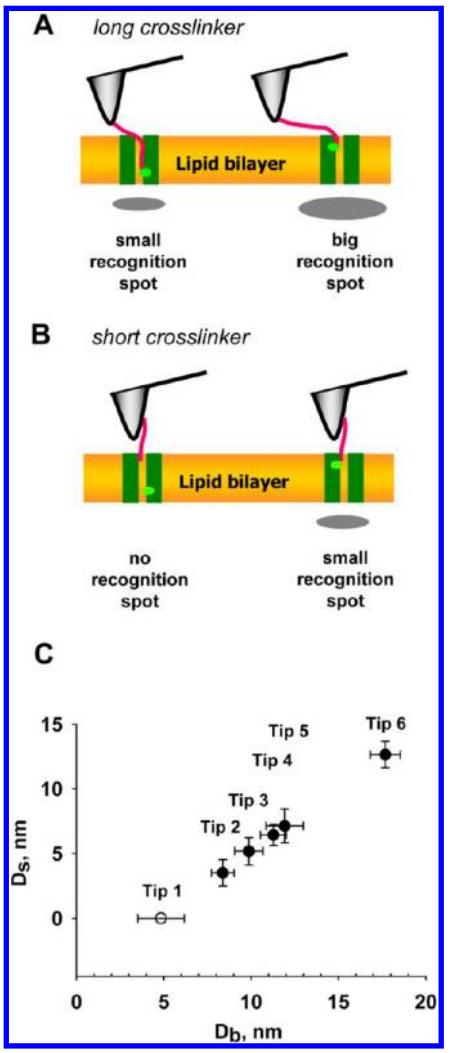

Figure 5. (A, B) Dependence of size of recognition spot on the orientation of UCP1 in the bilayer membrane and on the size of cross-linker. (C) Diameter of small (D_s) and large (D_b) recognition spots measured by six different cantilever tips.

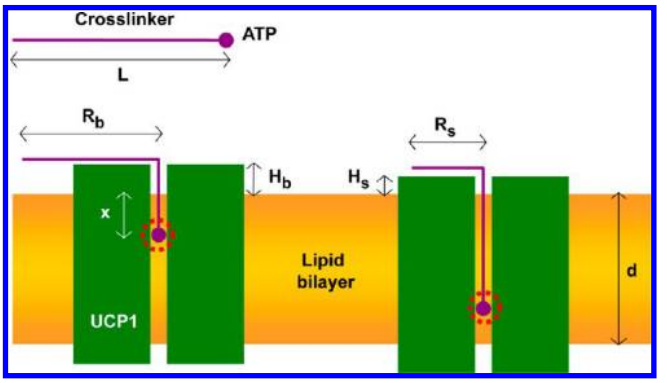

Figure 6. Scheme for the calculation of the nucleotide binding sites for different cantilever tips.

the crystallographic structure for UCP1, these data provide valuable insights into the mechanism of nucleotide binding.

■ EXPERIMENTAL SECTION

mUCP1 Expression, Purification, And Reconstitution into Liposomes. Murine uncoupling protein 1 (mUCP1) was produced as

dx.doi.org/10.1021/ja312550k | J. Am. Chem. Soc. XXXX, XXX, XXX–XXX

Table 1. Calculation of the Nucleotide Binding Sites for Different Cantilever Tips

	R_b (nm)	R_s (nm)	H_b (nm)	H_s (nm)	L (nm)	x (nm)
tip 1	2.42 ± 0.67					
tip 2	4.19 ± 0.33	1.77 ± 0.51	1.07 ± 0.23	0.99 ± 0.08	6.5	1.25
tip 3	4.93 ± 0.40	2.58 ± 0.53	1.50 ± 0.07	1.66 ± 0.33	7.8	1.40
tip 4	5.64 ± 0.37	3.22 ± 0.41	1.44 ± 0.17	1.13 ± 0.35	8.2	1.14
tip 5	5.96 ± 0.53	3.57 ± 0.65	0.75 ± 0.14	0.71 ± 0.19	8.0	1.28
tip 6	8.84 ± 0.43	6.33 ± 0.51	1.08 ± 0.13	1.20 ± 0.26	11.2	1.30
average			1.17 ± 0.31	1.14 ± 0.35		1.27 ± 0.1

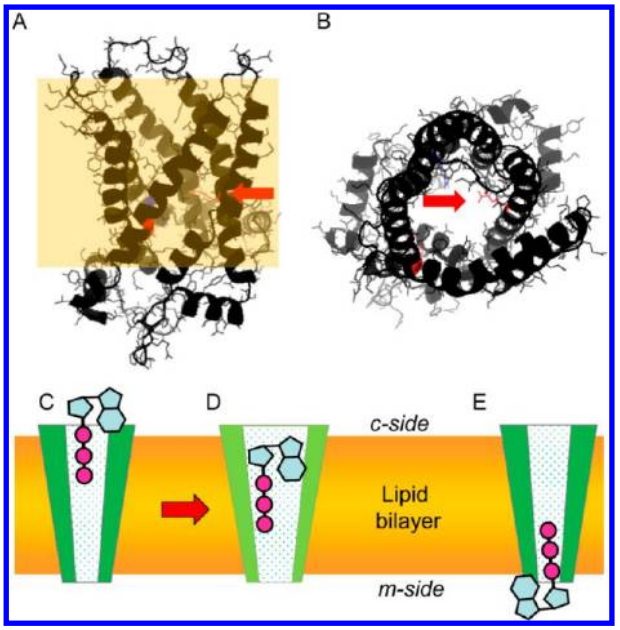

Figure 7. (A, B) Position of R182 in UCP1 visualized by PyMol. Proposed mechanism of ATP binding: initial binding from the c-side (C) followed by protein conformational change (D) and protein inhibition. (E) Protein binding from the m-side without conformational change and inhibition.

described previously.[15] The same batch of inclusion bodies was used for the protein reconstitution. Inclusion bodies (IB) containing UCP1 were purified, solubilized, and incorporated in liposomes according to established procedures.[12,15,29] Aggregated proteins were withdrawn by centrifugation of the dialysate at 14 000*g* for 10 min. To eliminate the incorrectly folded protein and nonionic detergent, the supernatant was added to a column containing 1 g of hydroxyapatite (Bio-Rad)[9,30] and the sample incubated with Bio-Beads SM-2 (Bio-Rad).[31] The protein content of the proteoliposomes was measured by a Micro BCA Protein Assay (Perbio Science).

Bilayers Reconstituted with UCP1 on Mica. The AFM sample plate (Agilent Technologies) with the coil for magnetic field application was covered with a small piece of aluminum foil, the center of which was marked by a small dot to indicate the cantilever position for the charge-coupled device (CCD) camera. Freshly cleaved mica was placed on the aluminum film and mounted with a flow-through fluid cell. Then 10−20 μL of UCP1 stock solution of proteoliposomes (with a lipid concentration of 4−5 mg/mL and a protein to lipid ratio of 0.02−0.03) was diluted with assay buffer (50 mM Na_2SO_4, 20 mM MES, 20 mM TRIS, 0.6 mM EDTA, pH 7.2) to a final volume of 250 μL. After short vortexing, the solution was injected into the fluid cell on the mica surface. After incubation for 8−10 min, the mica surface was thoroughly washed with buffer. Finally, 600 μL buffer was left in the fluid cell for measurements.

Cantilever Tip Modification. Magnetically coated cantilevers (MAC levers, Agilent) were functionalized with anti-UCP1 antibody or with the ethylenediamine derivative of ATP (EDA-ATP, 2′-/3′-*O*-(2-aminoethylcarbamoyl)-adenosine-5′-*O*-triphosphate, BioLog) by a well-established three-step procedure: (i) amino-functionalization of AFM tips by gas phase silanization with (3-aminopropyl)-triethoxysilane (APTES),[32] (ii) attachment of a heterobifunctional polyethylene glycol linker (NHS-PEG-aldehyde),[33] and (iii) reaction of the aldehyde function on the free end of the PEG chain with an amino group of the antibody or of EDA-ATP.[34]

To remove bovine serum albumin from commercially available anti-UCP1 antibody (Sigma), the latter was gel filtered on a Superdex-200 column (10 mm ×300 mm) in PBS (5 mM Na_2HPO_4, 150 mM NaCl, pH 7.5) at a flow rate of 0.5 mL/min. The IgG peak (0.2 mL) was collected and divided into 10 μL aliquots, which were frozen in liquid nitrogen and stored at −25 °C. For coupling to tip−PEG-aldehyde, several cantilever tips were placed into the 10 μL droplet of purified antibody. In the case of tip−PEG-acetal,[34] before the reaction with antibody the cantilevers were treated with 1% citric acid (pH2.2) for 10 min, washed three times in water and once in ethanol, and dried in air. Then, 1.2 μL of 0.2 M $NaCNBH_3$ [freshly prepared by dissolving 32 mg of $NaCNBH_3$ (Caution: toxic!) in a mixture of 50 μL of 100 mM NaOH plus 450 μL of water and diluting this stock solution with 2 mL of buffer A (100 mM NaCl, 50 mM NaH_2PO_4, 1 mM EDTA-Na_2, pH 7.5 adjusted with NaOH)] was mixed into the antibody solution, and the cantilever tips were incubated for 1 h. Subsequent optional deactivation of residual aldehyde functions on the tip was performed by addition of 0.5 μL of 1 M ethanolamine hydrochloride solution (preadjusted to pH 9.6 with NaOH and stored in small aliquots at −25 °C) and incubation for 10 min. The tips were washed and stored in buffer A at 4 °C before measurements.

AFM Imaging. Mac-mode AFM imaging was performed using a PicoPlus 5500 AFM (Agilent). Recognition images[35,36] were simultaneously recorded using the antibody- or ATP-functionalized cantilever, which was driven by an alternating magnetic field at its resonant frequency. Images were recorded at an amplitude set-point of 2.3−8.4 nm and with a ratio of 88−97% to the amplitude observed before the cantilever touched the sample surface. The scanning speed for imaging was 1.6−4 μm/s. Experiments on the blocking of ATP recognition were conducted by injecting free ATP solution into the measurement solution at a final concentration of 4.8 mM. Experiments on the blocking of the anti-UCP1 antibody recognition were conducted by injecting free peptide specific for the anti-UCP1 antibody into the measurement solution at a final concentration of about 20 μg/mL.

Data Analysis. Both topography and recognition images were displayed after leveling by mean plane subtraction and scanning line correction (Gwyddion 2.9). Membrane regions without protein were used to find the distribution of signal intensity in the recognition image. The minimum value was used as the threshold of recognition; i.e., only when the recognition signal was above the threshold was the protein considered to be recognized by the functionalized cantilever tip.

■ ASSOCIATED CONTENT

Supporting Information

Figure S1 shows high-resolution topography and recognition images of bilayer membrane without protein; Figure S2 shows topography and cross-section images for the estimation of the membrane thickness. This material is available free of charge via the Internet at http://pubs.acs.org.

dx.doi.org/10.1021/ja312550k | J. Am. Chem. Soc. XXXX, XXX, XXX−XXX

AUTHOR INFORMATION

Corresponding Author

elena.pohl@vedmeduni.ac.at

Notes

The authors declare no competing financial interest.

ACKNOWLEDGMENTS

This work was supported by Austrian Research Fund (FWF, P25357 to E.P. and SFB-F35 to R.Z. and P.H.). We are grateful to Barbara Unterauer and Philipp D. Pollheimer for purification of the antibody and to Dr. Graham Tebb for editorial assistance.

REFERENCES

(1) Mitchell, P. *Science* **1979**, *206* (4423), 1148−1159.
(2) Klingenberg, M.; Echtay, K. S. *Biochim. Biophys. Acta* **2001**, *1504* (1), 128−143.
(3) Nedergaard, J.; Ricquier, D.; Kozak, L. P. *EMBO Rep.* **2005**, *6* (10), 917−921.
(4) Lidell, M. E.; Enerback, S. *Nat. Rev. Endocrinol.* **2010**, *6* (6), 319−325.
(5) Cutting, W. C.; Mehrtens, H. G.; Tainter, M. L. *JAMA, J. Am. Med. Assoc.* **1933**, *101* (3), 193−195.
(6) Cannon, B.; Nedergaard, J. *Nature* **2012**, *488* (7411), 286−287.
(7) Harper, J. A.; Dickinson, K.; Brand, M. D. *Obes. Rev.* **2001**, *2* (4), 255−265.
(8) Nicholls, D. G.; Bernson, V. S.; Heaton, G. M. *Experientia Suppl* **1978**, *32*, 89−93.
(9) Lin, C. S.; Klingenberg, M. *FEBS Lett.* **1980**, *113* (2), 299−303.
(10) Nicholls, D. G. *Eur. J. Biochem.* **1976**, *62* (2), 223−228.
(11) Urbankova, E.; Voltchenko, A.; Pohl, P.; Jezek, P.; Pohl, E. E. *J. Biol. Chem.* **2003**, *278* (35), 32497−32500.
(12) Beck, V.; Jaburek, M.; Demina, T.; Rupprecht, A.; Porter, R. K.; Jezek, P.; Pohl, E. E. *FASEB J.* **2007**, *21* (4), 1137−1144.
(13) Krauss, S.; Zhang, C. Y.; Lowell, B. B. *Nat. Rev. Mol. Cell Biol.* **2005**, *6* (3), 248−261.
(14) Klingenberg, M. *Biochim. Biophys. Acta* **2010**, *1797* (6−7), 579−594.
(15) Rupprecht, A.; Sokolenko, E. A.; Beck, V.; Ninnemann, O.; Jaburek, M.; Trimbuch, T.; Klishin, S. S.; Jezek, P.; Skulachev, V. P.; Pohl, E. E. *Biophys. J.* **2010**, *98* (8), 1503−1511.
(16) Bouillaud, F.; Arechaga, I.; Petit, P. X.; Raimbault, S.; Levi-Meyrueis, C.; Casteilla, L.; Laurent, M.; Rial, E.; Ricquier, D. *EMBO J.* **1994**, *13* (8), 1990−1997.
(17) Modriansky, M.; Murdza, I. D.; Patel, H. V.; Freeman, K. B.; Garlid, K. D. *J. Biol. Chem.* **1997**, *272* (40), 24759−24762.
(18) Berardi, M. J.; Shih, W. M.; Harrison, S. C.; Chou, J. J. *Nature* **2011**, *476* (7358), 109−113.
(19) Pebay-Peyroula, E.; Dahout-Gonzalez, C.; Kahn, R.; Trezeguet, V.; Lauquin, G. J.; Brandolin, G. *Nature* **2003**, *426* (6962), 39−44.
(20) Klingenberg, M.; Winkler, E. *EMBO J.* **1985**, *4* (12), 3087−3092.
(21) Klingenberg, M. *Biochimie* **2007**, *89* (9), 1042−1048.
(22) Rial, E.; Nicholls, D. G. *FEBS Lett.* **1983**, *161* (2), 284−288.
(23) Dehez, F.; Pebay-Peyroula, E.; Chipot, C. *J. Am. Chem. Soc.* **2008**, *130* (38), 12725−12733.
(24) Wang, Y.; Tajkhorshid, E. *Proc. Natl. Acad. Sci. U. S. A* **2008**, *105* (28), 9598−9603.
(25) Palmieri, F. *Pflugers Arch.* **2004**, *447* (5), 689−709.
(26) Palmieri, F.; Pierri, C. L.; De, G. A.; Nunes-Nesi, A.; Fernie, A. R. *Plant J.* **2011**, *66* (1), 161−181.
(27) Kunji, E. R.; Robinson, A. J. *Curr. Opin. Struct. Biol.* **2010**, *20* (4), 440−447.
(28) Klingenberg, M. *Biochim. Biophys. Acta* **2008**, *1778* (10), 1978−2021.
(29) Jaburek, M.; Varecha, M.; Gimeno, R. E.; Dembski, M.; Jezek, P.; Zhang, M.; Burn, P.; Tartaglia, L. A.; Garlid, K. D. *J. Biol. Chem.* **1999**, *274* (37), 26003−26007.
(30) Lin, C. S.; Klingenberg, M. *Biochemistry* **1982**, *21* (12), 2950−2956.
(31) Rigaud, J. L.; Pitard, B.; Levy, D. *Biochim. Biophys. Acta* **1995**, *1231* (3), 223−246.
(32) Riener, C. K.; Stroh, C. M.; Ebner, A.; Klampfl, C.; Gall, A. A.; Romanin, C.; Lyubchenko, Y. L.; Hinterdorfer, P.; Gruber, H. J. *Anal. Chim. Acta* **2003**, *479*, 59−75.
(33) Ebner, A.; Wildling, L.; Kamruzzahan, A. S.; Rankl, C.; Wruss, J.; Hahn, C. D.; Holzl, M.; Zhu, R.; Kienberger, F.; Blaas, D.; Hinterdorfer, P.; Gruber, H. J. *Bioconjugate Chem.* **2007**, *18* (4), 1176−1184.
(34) Wildling, L.; Unterauer, B.; Zhu, R.; Rupprecht, A.; Haselgrubler, T.; Rankl, C.; Ebner, A.; Vater, D.; Pollheimer, P.; Pohl, E. E.; Hinterdorfer, P.; Gruber, H. J. *Bioconjugate Chem.* **2011**, *22* (6), 1239−1248.
(35) Stroh, C. M.; Ebner, A.; Geretschlager, M.; Freudenthaler, G.; Kienberger, F.; Kamruzzahan, A. S.; Smith-Gill, S. J.; Gruber, H. J.; Hinterdorfer, P. *Biophys. J.* **2004**, *87* (3), 1981−1990.
(36) Stroh, C.; Wang, H.; Bash, R.; Ashcroft, B.; Nelson, J.; Gruber, H.; Lohr, D.; Lindsay, S. M.; Hinterdorfer, P. *Proc. Natl. Acad. Sci. U. S. A* **2004**, *101* (34), 12503−12507.